Eur Biophys J (2011) 40:907–921
DOI 10.1007/s00249-011-0701-8

ORIGINAL PAPER

RNA dimerization monitored by fluorescence correlation spectroscopy

Arne Werner · Victor V. Skakun · Cindy Meyer · Ulrich Hahn

Received: 1 November 2010 / Revised: 2 March 2011 / Accepted: 18 March 2011 / Published online: 15 June 2011

Abstract Fluorescence correlation spectroscopy (FCS) provides a versatile tool to investigate molecular interaction under native conditions, approximating infinite dilution. One precondition for its application is a sufficient difference between the molecular weights of the fluorescence-labelled unbound and bound ligand. In previous studies, an 8-fold difference in molecular weights or correspondingly a 1.6-fold difference in diffusion coefficients was required to accurately distinguish between two diffusion species by FCS. In the presented work, the hybridization of two complementary equally sized RNA single strands was investigated at an excellent signal-to-noise ratio enabled by the highly photostable fluorophore Atto647N. The fractions of ssRNA and dsRNA were quantified by applying multicomponent model analysis of single autocorrelation functions and globally fitting several autocorrelation functions. By introducing a priori knowledge into the fitting procedure, 1.3- to 1.4-fold differences in diffusion coefficients of single- and double-stranded RNA of 26, 41, and 54 nucleotides could be accurately resolved. Global fits of autocorrelation functions of all titration steps enabled a highly accurate quantification of diffusion species fractions and mobilities. At a high signal-to-noise ratio, the median of individually fitted autocorrelation functions allowed a robust representation of heterogeneous data. These findings point out the possibility of studying molecular interaction of equally sized molecules based on their diffusional behavior, which significantly broadens the application spectrum of FCS.

Keywords Fluorescence correlation spectroscopy · dsRNA · Dimerization · Resolution

Abbreviations

AF	Autocorrelation function
bp	Base pair
dsRNA	Double-stranded RNA
FCS	Fluorescence correlation spectroscopy
FCCS	Fluorescence crosscorrelation spectroscopy
GAPDH	Glyceraldehyde-3-phosphate dehydrogenase
K_d	Dissociation constant
nt	Nucleotide
ssRNA	Single-stranded RNA

Introduction

Di- or even multimerization of ribonucleic acids (RNA) is widespread in nature, e.g., in the hybridization of complementary oligonucleotides in RNA interference (Jinek and Doudna 2009), in the life cycle of HIV (Paillart et al. 1996), or in protein kinase R activation (Andersen et al. 2004; Heinicke et al. 2009). The formation of RNA dimers

Electronic supplementary material The online version of this article (doi:10.1007/s00249-011-0701-8) contains supplementary material, which is available to authorized users.

A. Werner (✉) · C. Meyer · U. Hahn (✉)
Institute for Biochemistry and Molecular Biology, Department of Chemistry, Hamburg University, Hamburg, Germany
e-mail: arne_werner@web.de

U. Hahn
e-mail: uli.hahn@uni-hamburg.de

V. V. Skakun
Department of Systems Analysis, Faculty of Radio Physics and Electronics, Belarusian State University, Minsk, Belarus

or oligomers has been studied by various methods, e.g., UV melting (Ennifar et al. 2007; Riccelli et al. 1999) and analytical ultracentrifugation (Nakano et al. 2007). Fluorescence spectroscopy allows oligomerization to be studied in vitro and in vivo (Chen et al. 1999; Qian and Elson 1990). Double-strand formation of short RNA molecules has been found to be a hallmark of transcriptional and translational regulation (Farazi et al. 2008; Filipowicz et al. 2008). In the metabolism of short double-stranded RNA, various enzymes are involved. Fluorescence-based methods have enabled the formation of RNA double strands to be followed in complex environments. As biomolecules may artificially aggregate at high concentrations, methods that allow the oligomerization of RNA to be studied at nanomolar concentrations would be advantageous.

A fluorescence-based method that investigates hydrodynamic behavior under native conditions, approximating infinite dilution, is fluorescence correlation spectroscopy (FCS) (Ehrenberg and Rigler 1974; Magde et al. 1972). FCS monitors the diffusion of a fluorescence-labelled molecule through a confocal microscope detection volume of <1 fl. The interaction with a nonlabelled molecule can be identified by a change in mobility. It has been previously shown that an accurate quantification of the interaction of two binding partners requires at least an eightfold difference in molecular weight between the unbound and bound fluorescence species, which excludes the opportunity to monitor dimerization (Meseth et al. 1999). This limitation is not valid for fluorescence crosscorrelation spectroscopy (FCCS) (Eigen and Rigler 1994; Schwille et al. 1997). In FCCS experiments, two interacting molecule species are labelled by fluorophores with well separable emission spectra. The concomitant diffusion of the two species through the confocal volume can be monitored by crosscorrelating the signal of the corresponding detection channels. FCCS provides a robust method for interaction studies of equally sized molecule species, avoiding nonspecific binding to cellular components in vivo. However, to circumvent artefacts, a very careful calibration of a dual-color confocal laser set up is required (Bacia and Schwille 2007). In contrast, single-color FCS allows in vitro binding studies with relatively little calibration effort. Its resolution has been previously shown to depend on the signal-to-noise-ratio and fitting procedure (Meseth et al. 1999). In consideration of the constant progress in laser technology and fluorophore chemistry, we investigated the resolution of single-color FCS using Atto647N, a recently developed dye of high photostability and quantum yield (Eggeling et al. 2006). In the presented study, the biologically well defined system of the hybridization of short complementary RNA single strands is characterized by FCS, applying different fitting routines. Hydrodynamic models allowed us to estimate the role of the molecular shape and the degree of polymerization in the quantification of the fractions of two mobility species of molecular weights differing by a factor of 2.

Materials and methods

RNA

The RNA sequences were investigated for a 22 nucleotide (nt) RNA (5′-aag gcu gag aac ggg aag cuu u-3′) and the complementary 5′-Atto647N-labelled 26 nt RNA (5′-gaa aag cuu ccc guu cuc agc cuu ga-3′); a 41 nt RNA (5′-ccu uuc agc uca uuc cag gca ucc cuc uug gcc uug ccc ca-3′), modified at position 36 by Atto647N and at position 41 by Atto488 and the nonlabelled complementary strand; as well as a nonlabelled and 5′-Atto647N-labelled 54 nt RNA aptamer SRB2m (5′-gga acc ucg cuu cgg cga cga ugg gga ggc gca acg uua acc gcc uca ggu ucc-3′) (Holeman et al. 1998). The RNA was chemically synthesized and purified by denaturing polyacrylamide gel electrophoresis (PAGE) manufactured by IBA (Göttingen). The 22, 26, and 41 nt RNA sequences were derived from the human gene encoding glyceraldehyde-3-phosphate dehydrogenase (GAPDH).

The complementary nonlabelled 54 nt RNA was synthesized by in vitro transcription. Double-stranded DNA templates containing the T7 promotor were generated by hybridization of two complementary DNA oligonucleotides: AW1 (5′-aat gct aat acg act cact ata gga acc tga ggc ggt taa cgt tgc gcc tcc cca tcg tcg ccg aag cga ggt tcc-3′) und AW2 (5′-gga acc tcg ctt cgg cga cga tgg gga ggc gca acg tta acc gcc tca ggt tcc tat agt gag tcg tat tag catt-3′, Invitrogen; final concentration 1 μM). The two samples were mixed in equal amounts, heated to 80°C, and incubated for 5 min in PCR buffer [80 mM Tris-HCl, pH 8.8, 20 mM $(NH_4)_2SO_4$, 0.2% (w/v) Tween-20]. After cooling down to room temperature (RT), the resulting product was directly used for in vitro transcription by T7 RNA polymerase. For a 100 μl transcription reaction, 0.1 μM dsDNA, 1× transcription buffer (40 mM Tris-HCl, pH 7.9), 15 mM $MgCl_2$, NTPs (2.5 mM each), and 25 U T7 RNA polymerase were mixed, and the reaction was performed for 3 h at 37°C. The derived RNA was purified by 8% denaturing PAGE.

The RNA was diluted in buffer A (30 mM Tris-HCl, pH 6.8, 50 mM NaCl) and diethylpyrocarbonate (DEPC)-treated water to a final concentration of 1 μM. For hybridization titration experiments, in 12 different solutions of 50 or 100 μl final volume, 100 nM Atto647N-labelled 26 nt RNA and different amounts of nonlabelled 22 nt RNA were mixed. As control, only buffer A was added to the 26 nt RNA. Hybridization was performed by

heating for 3 min at 95°C, followed by cooling down to RT (1°C per 1.2 min) (modified from Kolb et al. 2005). Subsequently, $MgCl_2$ was added to a final concentration of 2.5 mM, followed by an incubation at RT for 30 min. For FCS measurements, the hybridized RNA solutions were diluted fourfold with buffer A, containing 2.5 mM $MgCl_2$. The concentration of the labelled RNA was determined by FCS. The concentration of the unlabelled RNA was determined by its optical density at 260 nm (Kibbe 2007). The labelled 41 nt RNA and 54 nt RNA were hybridized with different amounts of unlabelled complementary equally sized RNA as described for the 22 nt RNA and 26 nt RNA. FCS measurements of undiluted, 10-, and 100-fold diluted solutions were performed.

Fluorescence correlation spectroscopy

With FCS, the residence time τ_D of a fluorescent molecule in the detection volume V_{eff} of a confocal microscope can be determined (Magde et al. 1972). When measuring the fluorescence intensity fluctuations $\delta F(t)$ in the detection volume, τ_D is defined by the intensity-normalized autocorrelation function $G(\tau) = \langle \delta F(t+\tau)\delta F(t)\rangle / \langle F\rangle^2$. Assuming a spherical shape, the diffusion time depends on the molecular mass m with $\tau_D \propto \sqrt[3]{m}$.

FCS experiments were carried out using ConfoCor2 (Carl Zeiss Jena, Germany). The fluorophore Atto647N was excited at 633 nm with 2 or 3% of 5.0 mW of a HeNe laser, regulated by an acousto-optic tuneable filter (AOTF) using the C-Apochromat 40×, 1.2 NA, water immersion objective (Carl Zeiss, Jena, Germany). The emitted light was separated by a dichroic mirror HFT 633 nm and an emission filter LP 650 nm. The pinhole diameter was adjusted to 90 µm. The fluorescence signal was detected by an avalanche photodiode (SPCM-AQR-13-FC, Perkin Elmer). Experiments were performed at 22°C, and measurements lasted 30 × 1 s or 5 s. Evaporation of the sample was avoided with the use of a small cap. Using Zeiss software (4.0 SP2; R3.5) (Weisshart et al. 2004) or FCS Data Processor 2.0 program (Skakun et al. 2005), the fluorescence autocorrelation functions were fit to a model describing free three-dimensional diffusion and triplet excited state to determine the number of particles N, the diffusion time $\tau_{D,i}$, and the fractions f_i of n different diffusion species with $\sum f_i = 1$ (Weisshart et al. 2004) as follows:

$$G(\tau) = 1 + \frac{1}{N}\,\frac{1 - T + Te^{\frac{-\tau}{\tau_T}}}{(1-T)}\left(\sum_{i=1}^{n}\frac{f_i}{\left(1+\frac{\tau}{\tau_{D,i}}\right)\sqrt{1+\frac{\tau}{S^2\tau_{D,i}}}}\right). \quad (1)$$

The structure parameter S defines the ratio of the radial and axial distances between maximum and $1/e^2$ intensities of the focussed laser beam, r_0 and z_0. Signal fluctuations originating from singlet-triplet interaction are included in the fitting model by the decay time τ_T and the fractional population T. The parameters were derived from the Levenberg-Marquardt algorithm (Marquardt 1963). The reliability of the model was judged based on the χ^2 test and the residual deviations of the fit from the autocorrelation function.

When fractional populations of diffusion species are calculated, differences in the contribution of each diffusion species to the signal time trace have to be considered (Meseth et al. 1999). Assuming a mixture of two diffusion species with molecular brightness (cpm) η_1 and η_2 of diffusion species 1 and 2, respectively, the fractional population f_2 of diffusion species 2 was corrected as follows (Fradin et al. 2005):

$$f_{2'} = \frac{f_2\eta_2^2}{(1-f_2)\eta_1^2 + f_2\eta_2^2}. \quad (2)$$

Equation 2 was applied when η_1 and η_2 differed more than 1.1-fold.

To define the optical setup more accurately, the autocorrelation function of the standard fluorophor Cy5 was fitted using Origin software (Northampton, MA, USA):

$$G(\tau) = 1 + \frac{1}{N}\,\frac{1}{(1-T_1)(1-T_2)}\,(1 - T_1 + T_1 e^{\frac{-\tau}{\tau_{T1}}}) \times (1 - T_2 + T_2 e^{\frac{-\tau}{\tau_{T2}}})\frac{1}{\left(1+\frac{\tau}{\tau_{D,i}}\right)\sqrt{1+\frac{\tau}{S^2\tau_{D,i}}}}, \quad (3)$$

defining free three-dimensional diffusion, singlet-triplet transition, and an additional exponential decay, which is attributed to *cis-trans* isomerization (T_2, τ_{T2}) (Widengren and Schwille 2000). A structure parameter S of 6.3 ± 0.7 was found.

To calculate the diffusion coefficient D_i, r_0 was determined by referring to the diffusion time and diffusion coefficient of Cy5 [$D = 3.42 \times 10^{-10}$ m^2 s^{-1} at 295.15 K (Lemmon et al. 2011; Loman et al. 2008)] and applying

$$D_i = r_0^2/(4\tau_{D,i}), \quad (4)$$

and r_0 equal to 249 ± 7 nm was obtained. Knowing S and r_0, z_0 was calculated by applying

$$S = z_0/r_0. \quad (5)$$

The size of the effective detection volume V_{eff} for a three-dimensional Gaussian observation profile was calculated using

$$V_{\text{eff}} = \pi^{3/2} r_0^2 z_0, \quad (6)$$

and $V_{\text{eff}} \sim 0.5$ fl was obtained.

To reduce the risk of artefacts originating from changes in dimension and shape of the confocal detection volume (Enderlein et al. 2004), the sequence of the FCS measurements of the different solutions of a titration experiment was varied. ssRNA and dsRNA were measured consecutively. To balance changes in the shape of the confocal detection volume during the experiment, the structure parameter was kept unfixed in the fitting routine.

([ssRNA$_{_L_ub}$]) was defined by the concentration of total labelled ssRNA ([ssRNA$_{_L}$]) and fully hybridized dsRNA ([dsRNA]) according to the formula: [ssRNA$_{_L_ub}$] = [ssRNA$_{_L}$] − [dsRNA]. The dissociation constant K_d, given by $K_d = ([ssRNA_{\_NL\_ub}] \times [ssRNA_{\_L\_ub}])/[dsRNA]$, was determined by nonlinear regression analysis of the dependence of the fraction of dsRNA (f_{dsRNA}) on the concentration of total labelled and nonlabelled ssRNA ([ssRNA$_{_L}$] and [ssRNA$_{_NL}$]), respectively, by applying the formula:

$$f_{dsRNA} = \frac{K_d + [ssRNA_{\_L}] + [ssRNA_{\_NL}]) - \sqrt{(K_d + [ssRNA_{\_NL}] + [ssRNA_{\_L}])^2 - 4[ssRNA_{\_NL}][ssRNA_{\_L}]}}{2[ssRNA_{\_L}]}, \quad (7)$$

Global analysis of FCS data

With the use of the FCF Data Processor 2.0 software, parameters that are expected to have the same values through all fitted data sets can be linked (Skakun et al. 2005). Maximum and minimum limits of parameters can be introduced, and parameters known from independent measurements can be fixed. In a global analysis, several autocorrelation functions are analyzed simultaneously. Increasing the number of fitted autocorrelation functions increases the sensitivity and accuracy of the analysis while keeping the total number of parameters unchanged (Beechem et al. 1991). Initial guesses (IG) for the model parameters were generated by the phase plane method (Novikov et al. 1999) adapted to Eq. 1. The fit parameters were obtained based on the Marquardt-Levenberg nonlinear method of least squares (Marquardt 1963). The quality of the fit was judged by the χ^2 value and the residual deviations between experimental and fit curves. Confidence intervals of the recovered parameters were calculated as asymptotic standard errors at 67% confidence level. In the fitting routine, G_{inf} parameters were set fixed to 1.

Additional data analysis

Further data analysis was done with Excel (2005 Microsoft, Redmond, WA, USA) and Origin (Northampton, MA, USA).

In reference to Riccelli et al. (1999), the concentration of unbound nonlabelled ssRNA ([ssRNA$_{_NL_ub}$]) was defined by the concentration of total nonlabelled ssRNA ([ssRNA$_{_NL}$]) and fully hybridized dsRNA ([dsRNA]) according to the formula: [ssRNA$_{_NL_ub}$] = [ssRNA$_{_NL}$] − [dsRNA]. The concentration of unbound labelled ssRNA setting [ssRNA$_{_L}$] as fixed.

As a statistical measure for the goodness of the fit, the R^2 value was calculated with TSS, the total sum of squares, and RSS, the residual sum of squares:

$$R^2 = 1 - \frac{RSS}{TSS}. \quad (8)$$

Hydrodynamic models to predict translational diffusion

Double-stranded RNA typically shows an A-form geometry (Arnott et al. 1973; Varshavsky 2006). An equal hydrodynamic behavior of dsRNA and dsDNA was assumed. The translational diffusion coefficient of short dsDNA has been predicted by a theory of translational motion of cylinders (Fernandes et al. 2002; Tirado et al. 1984). The parameter A describes the ratio of the length L and the width d of a molecule as $2 < L/d < 30$ (for dsRNA this corresponds to 18 < base pairs < 250) according to the formula:

$$A = \ln(L/d) + 0.312 + 0.565/(L/d) - 0.1/(L/d)^2. \quad (9)$$

For dsRNA, a width of 26 Å (Ye et al. 2003) and an internucleotide distance of 2.9 Å/nt were set (Arnott et al. 1973). With parameter A, the Boltzmann constant κ (1.3807×10^{-23} kg m^2 s^{-2} K^{-1}), the viscosity η ($0.9544\ 10^{-3}$ kg m^{-1} s^{-1}; Lemmon et al. 2011), and the temperature T (295.15 K), the diffusion coefficient D of rod-like molecules was calculated:

$$D = A\kappa T/(3\pi\eta L). \quad (10)$$

The translational diffusion of spherical, globular molecules was calculated with the molecular mass m, the Avogadro constant N_A (6.023×10^{23} mol^{-1}), and the volumic mass of 1.8 g/cm^3 for nucleic acids (Voss and Gerstein 2005) in reference to van Holde et al. (1998):

$$R_H = \sqrt[3]{3m/(4\pi N_A \rho)}. \quad (11)$$

The molecular mass of the ribonucleic acids was determined assuming 321 g mol^{-1} per nucleotide (Kibbe 2007). By using the Stokes-Einstein equation, the hydrodynamic radius R_H was transformed into D:

$$D = \kappa T/(6\pi\eta R_H). \quad (12)$$

Considering RNA as homopolymer consisting of equally sized and freely rotating rigid units, the dependence of the diffusion coefficient D on the number of nucleotides N can be described in reference to Flory (1989):

$$D = aN^{-v}. \quad (13)$$

Results

Translational diffusion of 26 nt ssRNA and ~26 bp dsRNA

The translational diffusions of unhybridized single-stranded RNA (ssRNA) and hybridized double-stranded RNA (dsRNA) were compared. For this aim, Atto647N-labelled 26 nt ssRNA, solely or in the presence of saturating amounts of complementary nonlabelled 22 nt ssRNA ($[ssRNA_{NL}]/[ssRNA_L] = 6$), was re- and denatured, as described in "Materials and methods" (Fig. 1a). The autocorrelation function of dsRNA determined using FCS was slightly shifted to larger diffusion times in comparison to ssRNA (Fig. 1b). Both autocorrelation functions could be fit well to a model describing free three-dimensional diffusion of one diffusion species (Eq. 1 with $n = 1$). The structure parameter S was set fixed to a value that was determined in an independent experiment. Diffusion times, counts per molecule, triplet time, and triplet fraction of the experiments are summarized in Table 1. The small shift of the autocorrelation function corresponded to a 1.29-fold difference between ssRNA and dsRNA diffusion times, quantified as $1.30 \pm 0.01 \times 10^{-10}$ and $1.01 \pm 0.01 \times 10^{-10}$ m^2 s^{-1}, respectively. Due to the high photostability of Atto647N, we observed a small tendency to populate the triplet state, represented by a triplet fraction of 7–8%. The triplet fractions of ssRNA and dsRNA differed with a standard deviation of less than 1%. During the titration experiment, the triplet fraction changed over a standard deviation of 1–4%. The signal-to-noise ratio in FCS is predominantly defined by the molecular brightness, the measurement time, and the concentration (Koppel 1974; Qian 1990). In the presented experiment, an average molecular brightness of 65 kHz, overall measurement time

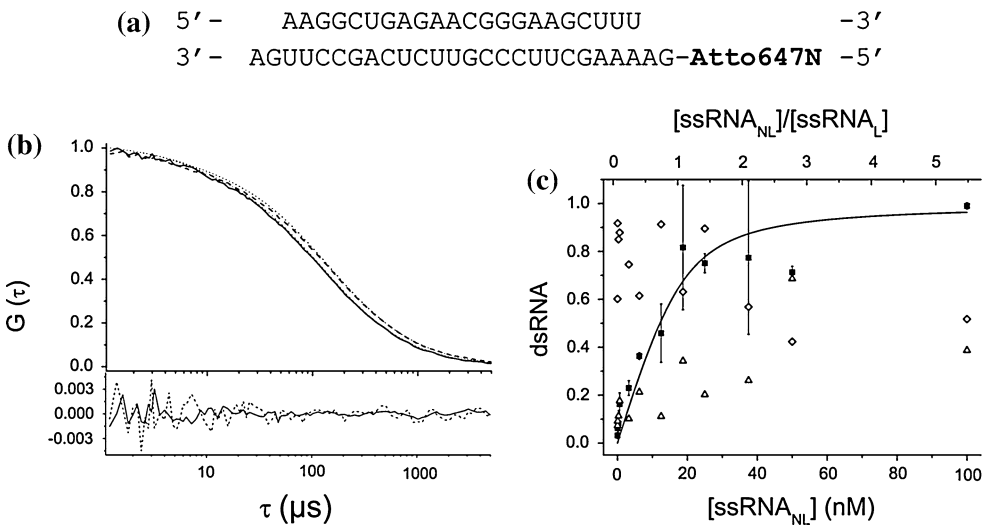

Fig. 1a–c Hybridization of complementary 22 and 26 nt ssRNA, investigated by multicomponent model analysis of averaged autocorrelation functions. **a** ssRNA and dsRNA sequences. **b** *Top* Experimentally determined autocorrelation functions (AFs) of Atto647N-labelled ssRNA (*solid line*) and Atto647N-labelled ssRNA after hybridization in the presence of saturating amounts of complementary nonlabelled ssRNA (dsRNA, *dashed line*, $[ssRNA_{NL}]/[ssRNA_L] = 6$). The data were fit to a model assuming one diffusion species according to Eq. 1 with $n = 1$ and fixed S (*dotted lines*). The autocorrelation values were normalized to unity at 1.2 µs. *Bottom* Residual deviations in the autocorrelation functions from the results of the fit. **c** Solutions containing a constant amount of Atto647N-labelled 26 nt ssRNA (18 nM) and different amounts of nonlabelled complementary 22 nt ssRNA were hybridized and measured by FCS for 5 s. The average of 30 autocorrelation functions was fitted. Data were analyzed by fitting to a model for two diffusion species without fixed diffusion time (*triangles*) or setting as fixed values one (τ_{D_ssRNA}, *diamonds*) or two diffusion times (τ_{D_ssRNA} and τ_{D_dsRNA}, *squares* and *line*) using Eq. 1 with $n = 2$. Mean values of two independent experiments were calculated. Standard deviations are shown for the fit with two fixed diffusion times. The fraction of dsRNA is plotted against the concentration of nonlabelled ssRNA and fit to Eq. 7, setting $[ssRNA_L]$ at a fixed amount (please see Table 2)

Table 1 Parameters of FCS measurements for ssRNA and dsRNA

	τ_D (μs)	D ($\times 10^{-10}$ m^2 s^{-1})	Cpm (kHz)	N	T (%)	τ_T (μs)
26 nt ssRNA	121 ± 4	1.30 ± 0.01	67 ± 19	6 ± 3	8.2 ± 0.3	8.0 ± 1.5
26 bp dsRNA	156 ± 6	1.01 ± 0.01	63 ± 12	8 ± 3	7.2 ± 0.1	6.1 ± 0.3
D_{ssRNA}/D_{dsRNA}		1.29				
41 nt ssRNA	151 ± 11	1.00 ± 0.01	61 ± 9	3.05 ± 0.03	4.7 ± 0.9	4.8 ± 1.7
41 bp dsRNA	199 ± 17	0.76 ± 0.01	69 ± 8	3.9 ± 0.3	4.5 ± 1.3	3.8 ± 0.4
D_{ssRNA}/D_{dsRNA}		1.31				
54 nt ssRNA	153 ± 10	0.961 ± 0.001	42 ± 11	9 ± 2	7.0 ± 0.9	10.1 ± 1.6
54 bp dsRNA	216 ± 32	0.69 ± 0.01	51 ± 16	3 ± 2	5.6 ± 0.2	6.1 ± 0.1
D_{ssRNA}/D_{dsRNA}		1.40				

τ_D Diffusion time, D diffusion coefficient, *cpm* counts per molecule, T triplet fraction, and τ_T triplet time of FCS measurements

Atto647N-labelled ssRNA (26, 41, and 54 nt) was hybridized in the presence of saturating amounts of nonlabelled complementary ssRNA ([$ssRNA_{NL}$]/[$ssRNA_L$] equal to 5 or 6). Measurements of 30 × 5 s were performed. The count rate was higher than 120 kHz. τ_D, cpm, N, T and τ_T were determined by a model for one diffusion species (Eq. 1 with $n = 1$). The diffusion coefficient was calculated using Eqs. 1, 3, and 4. Arithmetic mean and standard deviations of two independent experiments were calculated

of 5 min, and concentration of 18 nM defined a high signal-to-noise-ratio. The photophysical properties of the labelled ssRNA did not change significantly after hybridization. This allowed the fractions of the two mobility species to be accurately quantified by a two-component model analysis.

Hybridization of complementary 26 nt and 22 nt RNA single strands

To investigate complex formation, solutions containing a constant amount of labelled ssRNA and different amounts of complementary nonlabelled ssRNA were measured by FCS (see section "RNA"). Thirty individual autocorrelation functions, each with a measurement time of 5 s, were collected. An average of the autocorrelation functions was calculated and fit to a model of two diffusion species (Eq. 1 with $n = 2$). In the following, different fitting routines were applied to quantify the fractions of ssRNA and dsRNA.

Fixation of diffusion times in the fitting routine

It has been previously shown that by setting known parameters as fixed values in the fitting routine, the accuracy of the fit could be improved (Meseth et al. 1999; Rauer et al. 1996). As is described above, in independent experiments, the diffusion time of ssRNA was measured and determined by a model for one diffusion species. In additional independent experiments, the diffusion time of dsRNA was measured and determined by a model for one diffusion species. In the hybridization titration experiment, it was expected that mixtures of both diffusion species were present. Therefore, FCS data of the hybridization titration experiment were fitted by a model for two diffusion species. In addition, it was expected that the diffusion times of ssRNA and dsRNA were stable. To determine the effect of the fixation of the diffusion times, zero, one (ssRNA), or two (ssRNA and dsRNA) diffusion times were fixed to their previously determined values in the fitting routine. When fixing zero or one diffusion time, no physically significant dependence of the dsRNA fraction on the concentration of ssRNA resulted (Fig. 1c). When fixing two diffusion times in the fitting routine, the dependence of the dsRNA fraction on ssRNA concentration could be fitted to Eq. 7 with a correlation coefficient R^2 of 0.96. A dissociation constant of 3.2 ± 1.7 nM was obtained (Table 2).

Comparing the fit of the average of autocorrelation functions with the median of individually fitted autocorrelation functions

We further examined whether fitting several autocorrelation functions separately would reveal similar results compared to the fitting of the average of these curves. To determine how the population of fitting results could be most robustly represented, the distribution of the fraction of dsRNA obtained from fitting several autocorrelation functions was plotted in histograms for each titration step. Figure 2a, b show the titration steps of unhybridized and fully hybridized RNA whose dsRNA fractions were expected to be 0 and 1. In correspondence with the Poissonian distribution of single molecule data, a small number of fitting results was found to be outside of this range. The asymmetric distribution of the dsRNA fractions suggested using the median for a robust representation of the individually fitted autocorrelation functions. Setting two diffusion times as fixed values, the median of the fit of several autocorrelation functions deviated only to a minor extent

Table 2 Hybridization of 26 nt and complementary 22 nt dsRNA

Data analysis procedure	Experiments	K_d (nM)	R^2
Analysis of *n* single or averaged AFs by ConfoCor2 software			
Median results of 60 individually fitted AFs	2	3.4 ± 1.2[a]	0.92
Median results of 30 individually fitted AFs	2	3.3 ± 1.1[a]	0.93
Median results of 10 individually fitted AFs	2	2.1 ± 1.2[a]	0.89
Fit of the average of 30 AFs	2 × 1	3.2 ± 1.7[a]	0.96
Global analysis of *n* AFs of 12 titration steps by FCS Data Processor 2.0 software			
12 × 15 AF	2 × 1	4.1 ± 1.0[b]	0.96
12 × 10 AF	2 × 1	3.6 ± 1.0[b]	0.95
12 × 8 AF	2 × 1	3.7 ± 1.2[b]	0.93
12 × 5 AF	2 × 1	3.9 ± 1.1[b]	0.94

AF Autocorrelation function

Solutions with a constant fraction of Atto647N-labelled 26 nt ssRNA and different amounts of nonlabelled complementary 22 nt ssRNA ($[RNA_{NL}]/[RNA_L]$ of 0–6) were hybridized and measured by FCS. Data were analyzed by fitting to a model for two diffusion species with two fixed diffusion times (Eq. 1 with $n = 2$). The median of the fit results of *n* individually fitted autocorrelation functions of two independent experiments was calculated (Fig. 2). In comparison, the average of 30 autocorrelation functions of one titration experiment was fit, and mean value and standard deviation of the fit results of two independent titration experiments were calculated (Fig. 1). In addition, the results of the global analysis are presented (Fig. 3 and Supplementary Data Table S2). The global fit was performed setting the dsRNA fraction of ssRNA to 0 and of fully hybridized RNA to 1. The 12 titration steps, each represented by 5–15 autocorrelation curves, were globally analyzed with the FCS Data Processor 2.0 software. χ^2 criterion values of $\sim 2.94 \times 10^{-6}$ were introduced. The parameter groups of *S*, τ_{D_ssRNA}, τ_{D_dsRNA}, τ_T, and *T* and dsRNA fraction of *n* autocorrelation functions of one titration step were formed and linked, as they were expected to be constant. Then, the parameter groups of *S*, τ_{D_ssRNA}, τ_{D_dsRNA}, τ_T, and *T* of *n* autocorrelation functions of 12 titration steps were linked. Arithmetic mean and standard deviation of the fit results of two independent titration experiments were calculated. By nonlinear regression, the dependence of the dsRNA fraction on the concentration of the ssRNA was fit to Eq. 7, setting $[ssRNA_{NL}]$ fixed to 18 nM. The dissociation constant K_d was revealed in terms of the statistical accuracy using R^2 (Eq. 8)

[a] Fit, setting two diffusion times as fixed

[b] Fit, setting fraction 1 and 0 fixed

from the expected values. The median revealed 0.03 and 0.99 dsRNA. From the fit of the averaged autocorrelation functions, 0.07 and 1.00 dsRNA resulted. By fitting the median of the dsRNA fraction of all titration steps to Eq. 7, a K_d of 3.4 ± 1.2 nM was revealed (Fig. 2c; Table 2).

In the following, the accuracy of the fit results was investigated as a function of the number of repetitions of 5 s acquisitions, calculating the median from the fit results of the first 2–30 measurements of each of the two titration experiments, with a total of 4–60 measurements. The dsRNA fraction was plotted against the number of measurements and fitted to Eq. 7 (Fig. 2d; Table 2). Even the median dsRNA fraction of four single autocorrelation curves could be well fitted to Eq. 7 (Fig. 2d). In Fig. 2e, R^2 of the fit to Eq. 7 is plotted against the repetition number of 5 s measurements. The fixation of *S* in the fitting routine did not significantly increase R^2 (data not shown). The accuracy in the determination of the dissociation constant was relatively stable over 10–60 measurement repetitions. R^2 and K_d determined by the median of individually fitted autocorrelation functions corresponded to the R^2 and K_d determined from the arithmetic mean of an equal number of autocorrelation functions. In this titration experiment, at a concentration of 9 nM (cpm ~ 65 kHz), an overall collection time of 80 s (16 × 5 s) allowed for a robust quantification of the fractions of species whose diffusion times differed by 1.29-fold.

In addition, the opportunity to determine one diffusion time in a mixture of two diffusion species was investigated (Fig. 2f). When no parameters were fixed in a model for two diffusion species, the diffusion times were not in the range of the expected values (data not shown). Because diffusion time and *S* were correlated, ssRNA diffusion time and *S* were set fixed in the fitting routine. A dsRNA fraction of more than 50% was required for accurate dsRNA diffusion times. A comparable limitation was also observed for two- or fourfold mobility differences (data not shown).

Comparing the fit of single autocorrelation functions with the global fit of several autocorrelation functions

The accuracy of fit parameters of FCS data can largely be increased by a global analysis fitting several autocorrelation functions simultaneously and linking unaffected parameters (Beechem et al. 1991; Skakun et al. 2005). With the aim of judging the fit results of single autocorrelation functions, dsRNA hybridization titration experiments consisting of 12 measurements with different

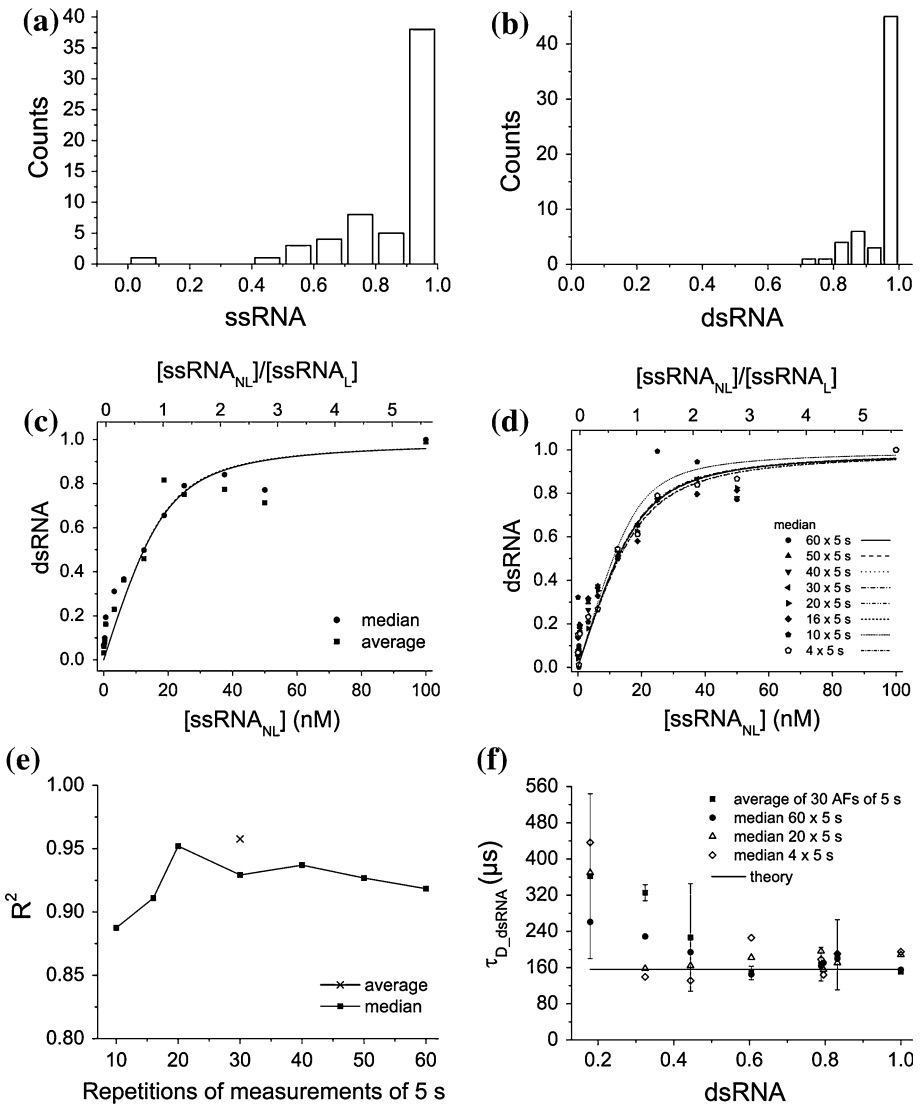

Fig. 2a–f Hybridization of complementary 22 and 26 nt ssRNA, investigating the distribution of the fit results of single autocorrelation functions. **a–e** FCS data were fitted to a model for two diffusion species with two fixed diffusion times using Eq. 1 with $n = 2$. Unhybridized (**a**) or fully hybridized labelled RNA (**b**) was measured 30×5 s in two independent experiments. Histograms of the fractions of ssRNA (**a**) and dsRNA (**b**) obtained by individually fitting 60 AFs to Eq. 1 are presented. **c** The dsRNA fraction was determined from the fit of the arithmetic mean of 30 AFs to Eq. 1, calculating arithmetic mean values of two independent experiments (*squares*). The median dsRNA fraction was calculated from 60 AFs individually fitted to Eq. 1, originating from two independent experiments (*circles*). The dependence of the dsRNA fraction on the concentration of nonlabelled ssRNA was fit to Eq. 7, yielding for the average and median dsRNA fraction a K_d of 3.2 ± 1.7 nM ($R^2 = 0.96$) and 3.4 ± 1.2 nM ($R^2 = 0.92$), respectively. **d** and **e** Variation in the measurement repetitions, counting from the first measurement of two independent experiments. **d** The median of dsRNA fractions of 4–60 AFs was fitted as a function of the concentration of nonlabelled ssRNA to Eq. 7 (please see Table 2). Corresponding R^2 values are shown in **e**. **f** Autocorrelation functions were fit to a model for two diffusion species setting S and one diffusion time fixed. Comparison of the diffusion time τ_{D_free}, which was determined experimentally in the titration steps, with τ_{D_dsRNA}, which was determined in a solution containing exclusively dsRNA, fitted to a model for one diffusion species

concentrations of nonlabelled ssRNA were globally analyzed. In the titration experiment, increasing amounts of nonlabelled ssRNA were added to a solution of a constant amount of labelled ssRNA. Therefore, the structure parameter S and the diffusion times of unhybridized and hybridized ssRNA should be constant in the different titration steps. Also triplet fraction T and triplet time τ_T were expected to be constant (Table 1). Therefore, the parameters S, τ_{D_ssRNA}, τ_{D_dsRNA}, τ_T, and T were linked (and corresponding parameter groups were formed) across all fitted autocorrelation functions from all titration steps. Additionally, in the different measurements of each titration step, the fraction of dsRNA should be the same. Then, dsRNA fractions of 15 autocorrelation functions of each titration step were linked, forming 12 additional parameter groups.

For an accurate quantification of the diffusion species fractions, the introduction of a priori knowledge was required. Two different strategies in fitting were studied. The first one introduced a priori knowledge about diffusion times obtained in the independent experiments (Supplementary Data Fig. S1 and Table S1). The second and most accurate one introduced a priori knowledge about the titration experiment scheme (no additional measurements were required). Minimum and maximum dsRNA fractions (corresponding to ssRNA and fully hybridized RNA) were set to 0 and 1 (Fig. 3 and Supplementary Data Table S2). The analysis of an equal number of single autocorrelation curves per titration step of two independent experiments did not allow the formation of all parameter groups due to variations in fit parameters. Therefore, two independent titration experiments were separately globally fitted, and arithmetic mean and standard deviation of the fit results were calculated (Fig. 3b). By fitting 5, 8, 10, or 15 autocorrelation functions per titration step, a comparable high accuracy in the dependence of the dsRNA fraction on [$ssRNA_{NL}$]/[$ssRNA_{L}$] was determined (Fig. 3c). The dissociation constant of the global study of 15 autocorrelation functions per titration step of 4.1 ± 1.0 nM is in the range of the K_d values of the individually fitted titration steps resulting from the analysis of several or averaged autocorrelation functions (Table 2). In comparison to the single fitted autocorrelation functions, for a similar statistical accuracy the global study required one-third of the overall acquisition time. In Fig. 3d, the diffusion times of the two mobility species in the titration experiment are compared with the independently determined diffusion times of ssRNA and dsRNA. Global fit results and the independently determined values agreed better than 1.03. This stands in strong contrast to the fit of single autocorrelation functions of individual titration steps (Fig. 2f).

Hybridization of complementary RNA single strands of 41 or 54 nt

The robustness of the resolution of the fractions of ssRNA and dsRNA in an undefined mixture was further investigated by FCS, studying RNA of different sequences and

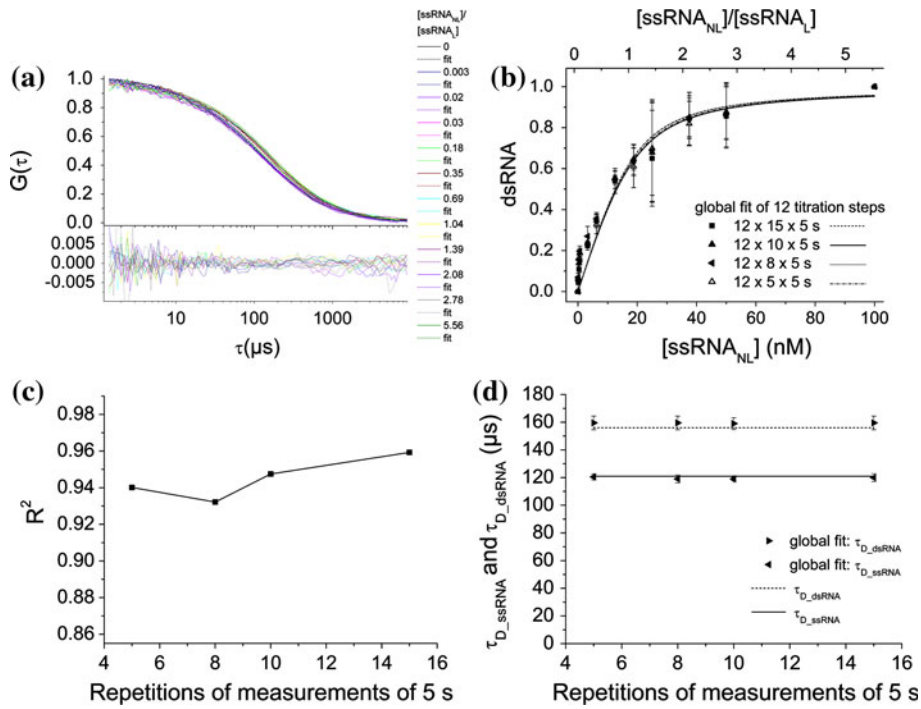

Fig. 3a–d Hybridization of complementary 22 and 26 nt ssRNA, globally fitted by the FCS Data Processor. The 12 titration steps of one experiment, each represented by 5, 8, 10, or 15 AFs, were globally analyzed with the FCS Data Processor 2.0 software. The global fit to Eq. 1 with $n = 2$ was performed by setting the dsRNA fraction of ssRNA to 0 and of fully hybridized RNA to 1. The parameter groups of S, τ_{D_ssRNA}, τ_{D_dsRNA}, τ_T, and T and dsRNA fraction of the 5–15 AFs of one titration step were formed and linked, as they were expected to be constant. Then, the parameter groups of S, τ_{D_ssRNA}, τ_{D_dsRNA}, τ_T, and T of 5–15 AFs of 12 titration steps were linked. χ^2 criterion values in the range of 2.65–2.94 × 10^{-6} were introduced. Confidence intervals (CI) were calculated as asymptotic standard errors at 67% level. The global fit results are further presented in Supplementary Data Table S2. **a** *Top* Experimentally determined autocorrelation functions (AFs) (*solid line*) and AFs resulting from the global fit to Eq. 1 with $n = 2$ (*dashed lines*) were normalized to unity at 1.4 μs. *Bottom* Residual deviations of the AFs from results of the fit. **b** The dsRNA fraction was fitted as a function of the concentration of nonlabelled ssRNA to Eq. 7 (please see Table 2). **c** R^2 of the fit to Eq. 7. **d** Diffusion times determined by the global fit of the 12 titration steps of 5–15 AFs to Eq. 1 with $n = 2$

length. For this aim, Atto647N-labelled 41 nt ssRNA was hybridized in the presence of different amounts of nonlabelled complementary 41 nt RNA. ssRNA and dsRNA were found to differ by 1.31-fold in their diffusion coefficients ($1.00 \pm 0.02 \times 10^{-10}$ vs. $0.76 \pm 0.01 \times 10^{-10}$ m^2 s^{-1}; Table 1 and Supplementary Data Fig. S2a). Solutions of different mixtures of both diffusion species were hybridized and measured by FCS. The data were analyzed by individually fitting 60 autocorrelation functions or the average of 30 autocorrelation functions to Eq. 1 with $n = 2$, setting two diffusion times as fixed values (Supplementary Data Fig. S2b). Fitting the dependence of the dsRNA fraction versus [$ssRNA_{\_NL}$] to Eq. 7 for the average and median, a K_d of 1.4 ± 0.5 and 1.0 ± 0.4 nM, respectively, was determined. The statistical accuracy of both analysis approaches was comparable. By varying the number of fitted AFs between 16 and 60 to calculate the median, the dissociation constants could be determined with comparable statistical accuracy (Supplementary Data Fig. S2c and d).

The resolution of different diffusion species by multicomponent model analysis depends on the signal-to-noise ratio (Meseth et al. 1999). It has been previously reported that the signal-to-noise ratio in FCS depends approximately linearly on the molecular brightness and on the square root of the measurement time (Koppel 1974). If the number of particles in the observation volume is smaller than ~ 10, the signal-to-noise ratio is significantly affected by the concentration (Qian 1990). To investigate the robustness of the differentiation between species differing in their diffusion times by 1.3-fold, in further experiments, the total RNA concentration was varied over three orders of magnitude. The acquisition time was set to 1 or 5 s. In Supplementary Data Fig. S2e, R^2 of the fit of the dsRNA fraction is presented as a function of [$ssRNA_{\_NL}$] according to Eq. 7 (Supplementary Data Table S3). A dependence of the resolution, which is defined by the signal-to-noise ratio, on measurement time and count rate (which is proportional to the concentration) is clearly visible. Median and average were equal at concentrations of 10–90 nM. Within the concentration range of 10–90 nM (42–66 kHz cpm) and 30 repetitions of 1 or 5 s measurements, fractions of species whose diffusion differed by 1.3-fold could be accurately quantified by multicomponent model analysis of single autocorrelation functions. At a concentration of 0.7 nM, with a count rate of 15 kHz, the average of 30 autocorrelation functions for collection times of 5 s, but not of 1 s could be fitted to Eq. 7. Furthermore, the median dsRNA fraction of individually fitted autocorrelation functions could not be accurately fitted to Eq. 7. These observations support the conclusion that at a low signal-to-noise ratio the averaging of autocorrelation functions and the increase in the acquisition time are advantageous to increase the accuracy of the fit. In contrast, a high signal-to-noise ratio allows the median of several individually fitted autocorrelation functions to be referenced, which opens the opportunity to exclude outliers. The global fits of 30 autocorrelation functions of 5 s per titration step allowed accurate results to be determined at concentrations ranging over three orders of magnitude.

In a second experiment, Atto647N-labelled 54 nt ssRNA, hybridized in the presence of different amounts of nonlabelled complementary 54 nt ssRNA was investigated by FCS (Supplementary Data Fig. S3). For 54 nt ssRNA and 54 bp dsRNA, diffusion coefficients of $0.961 \pm 0.001 \times 10^{-10}$ and $0.69 \pm 0.01 \times 10^{-10}$ m^2 s^{-1} were measured, respectively (Table 1 and Supplementary Data Fig. S3a). To balance the contribution of a 1.2-fold differing molecular brightness of ssRNA and dsRNA to the autocorrelation function, the fractional population of the diffusion species was corrected by applying Eq. 2 (Fradin et al. 2005). By fitting the arithmetic mean of 30 autocorrelation functions of two independent experiments and by choosing the median dsRNA fraction of the 60 individually fitted autocorrelation functions, a K_d of 0.99 ± 0.13 nM ($R^2 = 0.98$) and 0.77 ± 0.20 nM ($R^2 = 0.98$), respectively, was determined. Within the concentration range of 7–113 nM (35–58 kHz cpm) and 30 repetitions of 1 or 5 s acquisition time, fractions of species differing in their diffusion times by 1.4-fold could be accurately quantified by multicomponent model analysis of single autocorrelation functions (Supplementary Data Fig. S3c and d). At 113 nM and 5 s acquisition time, a sensitivity of the median to differences in cpm is visible. Global fits of 30 autocorrelation functions of 5 s per titration step allowed highly accurate results to be determined at concentrations between 0.2 and 113 nM.

Over concentration ranges of three orders of magnitude, the molecular brightness was relatively stable (Fig. 4). The impact of the measurement time on the resolution of species whose diffusion times differ by 1.3- and 1.4-fold was significant in all data analysis approaches at concentrations of ~ 1 nM. The fractions of species differing by 1.4-fold could be quantified with higher accuracy than the fraction of species differing by 1.3-fold at equal concentrations. This observation can be explained by the previously described dependence of the resolution on the difference in diffusion time (Meseth et al. 1999).

Discussion

1.3-fold difference in mobility

The resolution in the multicomponent model analysis of FCS was investigated by studying the biologically well

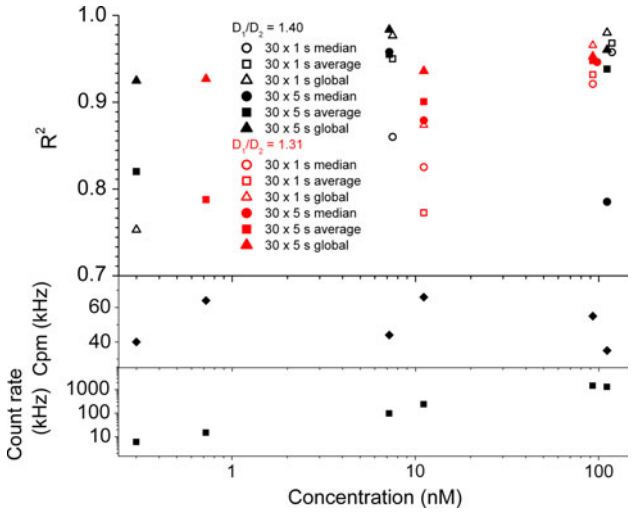

Fig. 4 Resolution of 1.3- and 1.4-fold differences in diffusion coefficients by FCS, depending on concentration and measurement time. Atto647N-labelled ssRNA of 41 or 54 nt was hybridized in the presence of saturating amounts of complementary nonlabelled ssRNA ($[ssRNA_{NL}]/[ssRNA_L]$ of up to 6). The mixtures of species differing in their diffusion by 1.3- or 1.4-fold were measured at different concentrations for 1 or 5 s. R^2 of the fit of the dsRNA fraction in relation to $[ssRNA_{NL}]$ according to Eq. 7 is presented. The dsRNA fraction resulted from the median fit result of 30 individually fitted AFs, the fit of the average of 30 AFs, or the global study of 30 AFs of nine titration steps

defined system of dsRNA hybridization. For 26, 41, and 54 nt RNA single strands, the hybridization with complementary nonlabelled RNA single strands was followed. The measured 1.3- and 1.4-fold differences in diffusion coefficients are in the range previously determined for a 25-bp dsDNA (Didier et al. 2009).

It has been shown that the resolution depends on the signal-to-noise ratio (Meseth et al. 1999), which itself strongly depends on the photophysical properties of the fluorophore and the measurement conditions (Koppel 1974; Qian 1990). To optimize the signal-to-noise ratio, the RNA was chemically labelled with Atto647N, a recently developed photostable dye of high quantum yield and extinction coefficient (Eggeling et al. 2006). A second strategy to improve the resolution was to apply advanced fitting routines (Beechem et al. 1991; Eigen and Rigler 1994; Skakun et al. 2005). The introduction of a priori knowledge into the fitting routine has been previously demonstrated to increase the accuracy of fit parameters (Meseth et al. 1999; Rauer et al. 1996). In a two-component model analysis, the fixation of both diffusion times to values determined in independent experiments allowed a highly accurate quantification of mobility species fractions. When fit results of different quality were compared, the risk of introducing artefacts by an insufficiently accurate fit became obvious. To distinguish between mobility species differing by a factor of 1.3–1.4, the introduction of prior knowledge into the fitting procedure was required. Even by global analysis, it was impossible to distinguish between one or two mobility species exclusively by statistical properties of experimental data. A precondition for the high resolution was either knowledge of the diffusion times of the individual mobility species or, preferentially, of the titration scheme.

A dependence of the signal-to-noise ratio on measurement time, cpm, and count rate or concentration, respectively, has been reported (Kask et al. 1997; Koppel 1974; Qian 1990). In the work presented here, at low signal-to-noise ratio, the averaging of autocorrelation functions allowed for increasing the information content of fit results. It has to be pointed out that the averaging of autocorrelation curves may introduce artefacts. Therefore in homogeneous solutions, the collection of data over long aquisition times should be preferred. Furthermore, we compared the parameters obtained by fitting the average of several autocorrelation functions with the median of the parameters obtained by individually fitting autocorrelation functions of equal number. Based on the corresponding results at high signal-to-noise ratio, we concluded that a system would be accurately represented if a large number of short measurement times were individually fitted. The median provides the opportunity to exclude outliers, which significantly increases the robustness of a study. This form of analysis might be advantageous in the heterogeneous environment of living cells, e.g., it might allow photobleaching artefacts to be avoided. The meaning of short acquisition times for the representation of heterogeneous systems has been pointed out (Saffarian and Elson 2003). To optimize measurement conditions that influence signal-to-noise, analytical equations have been derived (Kask et al. 1997; Saffarian and Elson 2003; Wohland et al. 2001).

By varying the number of acquisition repetitions when quantifying the fractions of species differing in their mobility by 1.3-fold by using the median, the minimum overall measurement time was estimated. At a molecular brightness of ~65 kHz, sixteen 5 s measurements were required when fitting single autocorrelation functions to obtain accurate mobility species fractions. By varying the concentration range over three orders of magnitude, fractions of species differing in their mobility by 1.3-fold were accurately quantified between ~7 and 100 nM by 30 repetitions of 1 or 5 s acquisition time. The global fit allowed an accurate resolution at ~1 nM in thirty 5 s acquisitions. For the fractions of species differing in their diffusion by 1.4-fold, a slightly higher resolution was reached.

In our investigation of how accurately diffusion times can be estimated in a system of two mobility species, exact diffusion times were difficult to determine in an undefined

mixture of two diffusion species by fitting single autocorrelation functions. In contrast, the global fit of the diffusion times determined by titration experiment, which differed from the independently measured values by less than 3%, showed a significant higher accuracy.

It was concluded that the global approach allowed for a higher accuracy in the differentiation between mobility species and for a higher robustness against variations in the signal-to-noise ratio than the fit of single autocorrelation functions. The high sensitivity of the global approach is related to the number of linked parameters. Consequently, a high stability of all linked parameters is required (variations must be only due to noise). The potential of the global approach will, therefore, be more sensitive to changes in optical parameters and to differences between model and data. The median result of individually fitted autocorrelation functions is more robust against deviations in the optical geometry that originate from long measurement series or independent experiments, as well as against heterogeneities in the investigated biological system. In heterogeneous data sets, therefore, at a high signal-to-noise ratio, the median is suggested for a robust data representation.

It has previously been reported that at least a 1.6-fold difference in diffusion coefficients is required for an accurate resolution of two species (Meseth et al. 1999). By fitting autocorrelation curves individually and globally, we found that fractions of two mobility species with a 1.3-fold difference in diffusion coefficients could be determined with high accuracy. Our study reports a significant improvement in the resolution of FCS. This progress might be explained by the high absorption coefficient, quantum yield, and photostability of Atto647N.

The high photostability of Atto647N allowed the signal-to-noise ratio to be maximized and the photophysical artefacts to be minimized (Eggeling et al. 2006). For the resolution of diffusion times differing by 1.3-fold, very stable conditions at the optical set up were an important precondition (see section "FCS"). When fitting autocorrelation functions to a model that assumes a three-dimensional Gaussian observation profile, deviations in the optical geometry may introduce errors in the fitted parameters (Enderlein et al. 2004). In addition, for the calculation of a diffusion coefficient, the dimensions of the confocal volume are estimated by a fluorophore of known diffusion coefficient. Therefore a second error source originates from differences between standard fluorophore and sample measurement conditions. With the introduction of an internal size standard in FCS measurements with the recently developed two-focus FCS, the robustness against refractive index mismatch, optical saturation, and deviations in other optical and photophysical factors could be significantly increased (Dertinger et al. 2008).

Twofold difference in molecular weight

A parameter that is more easily accessible than the diffusion time is the molecular weight, which often provides the basis to evaluate the feasibility of a single-color FCS experiment. Therefore, an exact knowledge of the minimum resolvable difference in molecular weight might be desired. In a previous study, the eightfold difference in molecular weight of a fluorophore and of bovine serum albumin were resolved (Meseth et al. 1999). The diffusion species investigated in our study differed in their molecular weights by a factor of 1.9 or 2. To answer whether the progress reported here might not only be explained by the excellent signal-to-noise ratio of the experiment, we investigated the role of the molecular shape in the resolution in FCS.

Molecular shape and hydrodynamic behavior of RNA

With X-ray diffraction analysis, dsRNA has been found to adopt an A-form geometry (Arnott et al. 1973; Ye et al. 2003). The hydrodynamic behavior of rod-shaped short double-stranded nucleic acids has been theoretically described as that of a rigid cylinder (Fernandes et al. 2002; Tirado et al. 1984) (please see also section "Hydrodynamic models to predict translational diffusion"). As a representation of maximally compact conformation, a spherical model was chosen. The diffusion coefficients of the ~26, 41, and 54 bp dsRNA agree with the model for cylinders (Fig. 5a). In contrast, due to the complexity of RNA single-stranded structures (Batey et al. 1999; Stombaugh et al. 2009), a theory for the dependence of the translational diffusion of evolutionarily unevolved ssRNA on the number of nucleotides does not yet exist. The diffusional behavior of the unhybridized evolutionarily unconserved ssRNA could be well approximated by the cylindrical model (Fig. 5a).

Diffusion coefficient ratios of monomer and dimer of cylindrical or spherical shape

To estimate the impact of the molecular shape on the differentiation between the diffusion times of equally sized molecules, we compared the dependence of the mobility of spherically formed molecules on the number of nucleotides with that of rod-like molecules, applying Flory's law on the dependence of the diffusion coefficient D on the unit number N, $D \sim N^{-\nu}$ (Flory 1989). The exponent ν depends on the solubility of the polymer, ranging from three-fifths to one-third. For molecules of maximally compact conformation, ν is expected to be 0.33. An exponent of 0.57 has previously been determined for short dsDNA (Robertson et al. 2006). We applied the power law

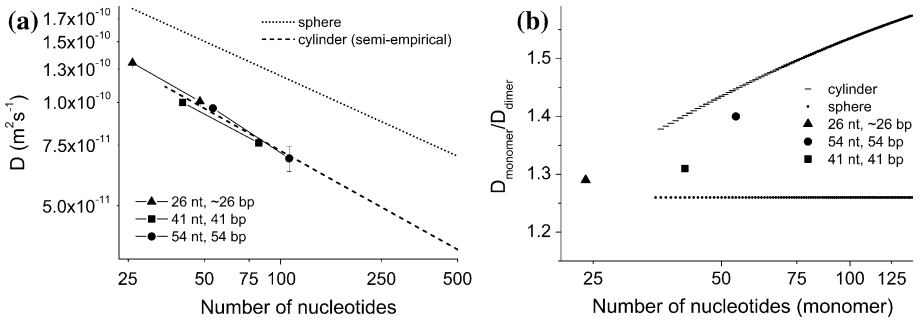

Fig. 5a, b Single- and double-stranded RNA diffusion time as a function of the number of nucleotides. **a** All hydrodynamic data are presented as described in the legend. Diffusion coefficients of cylindrically shaped dsRNA were calculated using Eqs. 9 and 10. Diffusion coefficients of spherically shaped RNA were predicted applying Eqs. 11 and 12. To facilitate the comparison of different models, the number of base pairs used in the cylindrical model is represented as doubled nucleotide number. The dependence of the diffusion coefficient D on the number of nucleotides N was fit to Eq. 13. By applying the cylindrical model, $D = 9.7 \times 10^{-10}$ $N^{-0.61}$ m^2 s^{-1} (35–500 nt, *dashed line*) was obtained, and by applying the spherical model, $D = 5.56 \times 10^{-10}$ $N^{-0.33}$ m^2 s^{-1} (26–500 nt, *dotted line*) was obtained. Experimental data of the hybridization of complementary 22 and 26 nt ssRNA are shown as *squares*, complementary 41 nt ssRNA as *triangles*, complementary 54 nt ssRNA as *filled circles*. **b** Dimerization is represented by the ratios of the diffusion coefficients of monomer and dimer. The ratio of diffusion coefficients was calculated for dsRNA of 18–250 bp with the cylindrical model (*lines*) and for ssRNA of 26–500 nt with the spherical model (*circles*). The experimentally determined ratios of the diffusion coefficients of monomer and dimer are presented in analogy to **a**

on the hydrodynamic models of cylinder and sphere, which refer to the physicochemical properties of RNA. Exponents of 0.61 for cylindrically formed dsRNA of 18–250 bp and of 0.33 for spherically formed RNA were obtained, in agreement with literature values (Fig. 5a). By comparing the exponents 0.6 and 0.3, it was concluded that, in FCS experiments, a significantly higher resolution of molecular weight differences can be reached for cylindrically formed molecules in comparison to spheres.

In the following, resolution differences of sphere and cylinder were quantified considering dimerization. The diffusion coefficients of ribonucleic acids were each divided by the diffusion coefficient of an oligonucleotide of doubled nucleotide number. The spherical model gave a constant value of 1.26 for $D_{monomer}/D_{dimer}$ (D_1/D_2), simplifying Eq. 12 to $D_1/D_2 = 2^{1/3}$. For the cylindrical model, D_1/D_2 increased from 1.37 to 1.64 and resembled a hyperbola (Fig. 4b). This observation can be explained by Eq. 10, in this case $D_1/D_2 = (2 \times A_1)/A_2$. In this model D_1/D_2 solely depends on A, a parameter related to the ratio of diameter and length of the molecule. We concluded that the resolution of a dimerization of perfectly spherical molecules, representing a maximally compact conformation, does not depend on the polymer length. In contrast, an increase in asphericity leads to an increase in the ratio of monomer and dimer diffusion coefficients.

Shape effects on the resolution of RNA dimerization by translational diffusion

Due to the correspondence of ssRNA and dsRNA mobility with the cylindrical model, an increase in D_1/D_2 with polymer size was observed (Fig. 5b). The deviation from the cylindrical model may predominantly result from heterogeneities in the conformation of the ssRNA. For dsRNA hybridization, the resolution of a dimerization by diffusion velocity seems to be facilitated by the cylindrical shape of monomer and dimer.

A dimerization-induced compaction may significantly influence the ratio of the diffusion velocity of both mobility species.

It has to be pointed out that by applying two-focus FCS, 1.2-fold differences in molecular weight could be resolved by translational diffusion measurements (Didier et al. 2009).

Conclusions

The study presented here demonstrates that the resolution limit of FCS is significantly lower than so far assumed. It has been previously determined that a 1.6-fold difference in translational diffusion coefficients is necessary to quantify the fractions of two mobility species. Using Atto6457N, a fluorophore with a high absorption coefficient, quantum yield, and photostability, and introducing a priori knowledge in the routine of individual or global fits of autocorrelation functions, 1.3- to 1.4-fold mobility differences could be resolved with high accuracy.

The measurement conditions were varied concerning concentration, acquisition time, and measurement repetitions. Measuring 30 repetitions of a 1 or 5 s acquisition over a concentration range of ~10–110 nM, the fractions of species differing in their mobility by 1.3- or 1.4-fold

could be accurately quantified by fitting single autocorrelation functions. When comparing the fit result of the average of several autocorrelation functions and the median result of individually fitted autocorrelation functions, no difference was found at a high signal-to-noise ratio, while at a low signal-to-noise ratio the averaging of autocorrelation functions was advantageous. With the precondition of a high signal-to-noise ratio, the median of individually fitted autocorrelation functions provides the possibility to exclude outliers and is suggested as a robust representation of heterogeneous data.

The global fit of several autocorrelation curves of one titration experiment reached a significantly higher accuracy in quantifying mobility species fractions and diffusion times than the fit of single autocorrelation functions, requiring one-third of the overall measurement time. Global fitting was found to be more robust against variations in the signal-to-noise ratio. The required stability of linked parameters limited the robustness against heterogeneities in experimental parameters or the investigated biological system. In the titration experiments, the fit of single autocorrelation functions depended to a larger extent on the signal-to-noise ratio but was less affected by variations in fit parameters.

It was further found that the molecular shape of monomer and dimer affects the translational diffusion velocity ratio. In terms of a hydrodynamic model for rigid cylinders, an increase in asphericity led to an increase in the ratio of monomer and dimer diffusion coefficients.

In our investigation of the hybridization of 26, 41, and 54 bp dsRNA twofold differences in molecular weight could be resolved by FCS. The results of our study point out the possibility of applying FCS in vitro on binding studies in which unbound and bound ligands differ to a relatively small extent in their molecular weights.

Acknowledgments We thank Johan Strömqvist for his advice in nonlinear regression analysis.

References

Andersen ES, Contera SA, Knudsen B, Damgaard CK, Besenbacher F, Kjems J (2004) Role of the trans-activation response element in dimerization of HIV-1 RNA. J Biol Chem 279:22243–22249

Arnott S, Hukins DW, Dover SD, Fuller W, Hodgson AR (1973) Structures of synthetic polynucleotides in the A-RNA and A′-RNA conformations: X-ray diffraction analyses of the molecular conformations of polyadenylic acid polyuridylic acid and polyinosinic acid polycytidylic acid. J Mol Biol 81:107–122

Bacia K, Schwille P (2007) Practical guidelines for dual-color fluorescence cross-correlation spectroscopy. Nat Protoc 2:2842–2856

Batey RT, Rambo RP, Doudna JA (1999) Tertiary motifs in RNA structure and folding. Angew Chem Int Ed 38:2326–2343

Beechem JM, Gratton E, Ameloot M, Knutson J, Brand L (1991) The global analysis of fluorescence intensity and anisotropy decay data: second-generation theory and programs. In: Lakowicz J (ed) Topics in fluorescence spectroscopy, vol 2. Plenum, New York, pp 241–305

Chen Y, Müller JD, So PTC, Gratton E (1999) The photon counting histogram in fluorescence fluctuation spectroscopy. Biophys J 77:553–567

Dertinger T, Loman A, Ewers B, Muller CB, Kramer B, Enderlein J (2008) The optics and performance of dual-focus fluorescence correlation spectroscopy. Opt Express 16:14353–14368

Didier P, Godet J, Mely Y (2009) Two-photon two-focus fluorescence correlation spectroscopy with a tunable distance between the excitation volumes. J Fluoresc 19:561–565

Eggeling C, Widengren J, Brand L, Schaffer J, Felekyan S, Seidel CAM (2006) Analysis of photobleaching in single molecule multicolor excitation and Förster resonance energy transfer measurements. J Phys Chem A 110:2979–2995

Ehrenberg M, Rigler R (1974) Rotational Brownian motion and fluorescence intensity fluctuations. Chem Phys 4:390–401

Eigen M, Rigler R (1994) Sorting single molecules: application to diagnostics and evolutionary biotechnology. Proc Natl Acad Sci USA 91:5740–5747

Enderlein J, Gregor I, Patra D, Fitter J (2004) Art and artefacts of fluorescence correlation spectroscopy. Curr Pharm Biotech 5:155–161

Ennifar E, Bernacci S, Wolff P, Dumas P (2007) Influence of C-5 halogenation of uridines on hairpin versus duplex RNA folding. RNA 13:1445–1452

Farazi TA, Juranek SA, Tuschl T (2008) The growing catalog of small RNAs and their association with distinct Argonaute/Piwi family members. Development 135:1201–1214

Fernandes MX, Ortega A, Lopez Martinez MC, García de la Torre J (2002) Calculation of hydrodynamic properties of small nucleic acids from their atomic structure. Nucleic Acids Res 30:1782–1788

Filipowicz W, Bhattacharyya SN, Sonenberg N (2008) Mechanisms of post-transcriptional regulation by microRNAs: are the answers in sight? Nat Rev Genet 9:102–114

Flory P (1989) Statistical mechanics of chain molecules. Hanser, Munich

Fradin C, Zbaida D, Elbaum M (2005) Dissociation of nuclear import cargo complexes by the protein Ran: a fluorescence correlation spectroscopy study. C R Biol 328:1073–1082

Heinicke LA, Wong CJ, Lary J, Nallagatla SR, Diegelman-Parente A, Zheng X, Cole JL, Bevilacqua PC (2009) RNA dimerization promotes PKR dimerization and activation. J Mol Biol 390:319–338

Holeman LA, Robinson SL, Szostak JW, Wilson C (1998) Isolation and characterization of fluorophore-binding RNA aptamers. Fold Des 3:423–431

Jinek M, Doudna JA (2009) A three-dimensional view of the molecular machinery of RNA interference. Nature 457:405–412

Kask P, Günther R, Axhausen P (1997) Statistical accuracy in fluorescence fluctuation experiments. Eur Biophys J 25:163–169

Kibbe W (2007) OligoCalc: an online oligonucleotide properties calculator. Nucleic Acids Res 35:W43–W46. doi: 10.1093/nar/gkm234

Kolb F, Zhang H, Jaronczyk K, Tahbaz N, Hobman T, Filipowicz W (2005) Human dicer: purification, properties, and interaction with PAZ PIWI domain proteins. Methods Enzym 392:316–336

Koppel DE (1974) Statistical accuracy in fluorescence correlation spectroscopy. Phys Rev A 10:1938–1945

Lemmon E, McLinden M, Friend D (2011) Thermophysical properties of fluid systems, vol 69. National Institute of Standards and Technology, Gaithersburg

Loman A, Dertinger T, Koberling F, Enderlein J (2008) Comparison of optical saturation effects in conventional and dual-focus fluorescence correlation spectroscopy. Chem Phys Lett 459:18–21

Magde D, Elson E, Webb WW (1972) Thermodynamic fluctuations in a reacting system—measurement by fluorescence correlation spectroscopy. Phys Rev Lett 29:705–708

Marquardt D (1963) An algorithm for least squares estimation of nonlinear parameters. J Soc Ind Appl Math 11:431–441

Meseth U, Wohland T, Rigler R, Vogel H (1999) Resolution of fluorescence correlation measurements. Biophys J 76:1619–1631

Nakano S, Kirihata T, Fujii S, Sakai H, Kuwahara M, Sawai H, Sugimoto N (2007) Influence of cationic molecules on the hairpin to duplex equilibria of self-complementary DNA and RNA oligonucleotides. Nucleic Acids Res 35:486–494

Novikov E, van Hoek A, Visser A, Hofstraat J (1999) Linear algorithms for stretched exponential decay analysis. Opt Commun 166:189–199

Paillart J, Marquet R, Skripkin E, Ehresmann C, Ehresmann B (1996) Dimerization of retroviral genomic RNAs: structural and functional implications. Biochimie 78:639–653

Qian H (1990) On the statistics of fluorescence correlation spectroscopy. Biophys Chem 38:49–57

Qian H, Elson EL (1990) On the analysis of high order moments of fluorescence fluctuations. Biophys J 57:375–380

Rauer B, Neumann E, Widengren J, Rigler R (1996) Fluorescence correlation spectrometry of the interaction kinetics of tetramethylrhodamin a-bungarotoxin with Torpedo californica acetylcholine receptor. Biophys Chem 58:3–12

Riccelli PV, Vallone PM, Kashin I, Faldasz BD, Lane MJ, Benight AS (1999) Thermodynamic, spectroscopic, and equilibrium binding studies of DNA sequence context effects in six 22-base pair deoxyoligonucleotides. Biochemistry 38:11197–11208

Robertson RM, Laib S, Smith DE (2006) Diffusion of isolated DNA molecules: dependence on length and topology. Proc Natl Acad Sci USA 106:7310–7314

Saffarian S, Elson EL (2003) Statistical analysis of fluorescence correlation spectroscopy: the standard deviation and bias. Biophys J 84:2030–2042

Schwille P, Meyer-Almes F-J, Rigler R (1997) Dual-color fluorescence cross-correlation spectroscopy for multicomponent diffusional analysis in solution. Biophys J 72:1878–1886

Skakun VV, Hink MA, Digris AV, Engel R, Novikov EG, Apanasovich VV, Visser AJWG (2005) Global analysis of fluorescence fluctuation data. Eur Biophys J 34:323–334

Stombaugh J, Zirbel CL, Westhof E, Leontis NB (2009) Frequency and isostericity of RNA base pairs. Nucleic Acids Res 37:2294–2312

Tirado MM, Martinez CL, García de la Torre J (1984) Comparism of theories for the translational and rotational diffusion coefficients of rod-like macromolecules. Applications to short DNA fragments. J Chem Phys 81:2047–2052

van Holde KE, Johnson WE, Ho PS (1998) Principles of physical biochemistry. Prentice-Hall, New Jersey

Varshavsky A (2006) Discovering the RNA double helix and hybridization. Cell 127:1295–1297

Voss NR, Gerstein M (2005) Calculation of standard atomic volumes for RNA and comparison with proteins: RNA is packed more tightly. J Mol Biol 346:477–492

Weisshart K, Jüngel V, Briddon SJ (2004) The LSM 510 META-ConfoCor 2 system: an integrated imaging and spectroscopic platform for single-molecule detection. Curr Pharm Biotech 5:135–154

Widengren J, Schwille P (2000) Characterization of photoinduced isomerization and back-isomerization of the cyanine dye Cy5 by fluorescence correlation spectroscopy. J Phys Chem 104:6416–6428

Wohland T, Rigler R, Vogel H (2001) The standard deviation in fluorescence correlation spectroscopy. Biophys J 80:2987–2999

Ye K, Malinina L, Patel DJ (2003) Recognition of small interfering RNA by a viral suppressor of RNA silencing. Nature 426:874–878